Journal of Solid Mechanics Vol. 17, No. 1 (2025) pp. 75-97
DOI: 10.60664/jsm.2025.1187928

Research Paper

Mixed-Mode Transient Analysis of Multiple Interface Cracks Between Half-Plane and Functionally Graded Layer

M. Rezaei Rased [1], R. Bagheri [1 *], R. Jamalpour [2]

[1] *Department of Mechanical Engineering, Karaj Branch, Islamic Azad University, Karaj, Iran*
[2] *Department of Civil Engineering, Karaj Branch, Islamic Azad University, Karaj, Iran*

Received 22 October 2024; Received in revised form 23 February 2025; Accepted 23 February 2025

ABSTRACT

The propagation of multiple interfacial cracks in dissimilar materials under mixed-mode impact loading conditions is investigated in this study. The analytical framework utilized in this investigation is rooted in the distributed dislocation technique. The method of integral transformations is employed to compute stress fields within a medium containing dislocations, positioned at the interface boundary between the half-plane and the functionally graded layer. Dislocation solutions are employed to formulate systems of Cauchy singular integral equations to characterize the traction vector along the surfaces of cracks. These integral equations are solved numerically to determine the dislocation density along the crack surfaces. This information allows for the computation of dynamic stress intensity factors (DSIFs) at the crack tips. The numerical results illustrate the impact of nonhomogeneity parameters, coating thickness, crack length, and interactions between cracks on DSIFs. These findings provide valuable insights into the behavior of graded coatings under impact loads.

Keywords: Multiple interface crack; Functionally graded coatings; In-plane loading; Dynamic stress intensity analysis; Dislocation technique.

1 INTRODUCTION

THE materials research community is actively exploring the application of functionally graded materials (FGMs) as surface coatings in diverse technological contexts. These coatings, featuring graded material compositions, are primarily designed for use as thermal, wear-resistant, or friction-reducing coatings, as well as interlayers within various technological applications. A notable challenge observed in FGM coating applications is the occurrence of

* Corresponding author. Tel.: +98 912 661 6721.
E-mail address: r.bagheri@kiau.ac.ir (R. Bagheri)

JOURNAL OF SOLID MECHANICS JSM

delamination, where cracks originating at the interface lead to the detachment of the FGM coating from the substrate. Hence, the comprehensive examination of fracture mechanics within engineering materials, where FGMs are employed as coatings, and the precise computation of stress intensity factors associated with interface cracks, are vital aspects in the endeavor to design secure bi-material structures. It is worth noting that the intricacy involved in solving the governing differential equations for FGMs arises from the necessity of using variable coefficients, rather than constants, underscoring the complexity of this analytical challenge. Currently available articles on the fracture behavior of FGMs predominantly focus on static mixed-mode or quasi-static problems.Numerous researchers have dedicated substantial efforts to investigate the static fracture behavior of interface cracks in graded coatings under mixed-mode conditions[1-8]. Cracked structures composed of Functionally Graded Materials (FGMs) often operate under critical conditions, exposed to impact loads. Consequently, it becomes imperative to thoroughly explore the dynamic fracture behavior of layered nonhomogeneous structures that encompass interfacial cracks. Guo et al. [9] conducted a study on the dynamic fracture behavior of a functionally graded coating-substrate system. The study involved examining a system with a crack perpendicular to the material interface under the influence of in-plane transient loading conditions. Guo et al. [10] explored the dynamic behavior of a functionally graded coating-substrate system that included either an internal crack or a transverse crack oriented normal to the interface. In their research, Guo et al. [11] delved into the dynamic analysis of a layered structure featuring a cracked FGM strip, all while being subjected to an impact load. This investigation focused on examining the influences of material nonhomogeneity values and geometric parameters on the DSIFs. Yong Dong et al. [12] developed a mechanical model to address the dynamic fracture problem associated with a weak-discontinuous interface between an FGM coating and an FGM substrate. They derived the Cauchy singular integral equation for the crack using integral transform techniques and employed an allocation method to obtain a numerical solution for the problem. Guo and Noda [13] conducted an analysis on the dynamic response of an FG composite that included a crack traversing the interface. They employed techniques such as Laplace and Fourier integral transforms, the singular integral equation method, and residue theory to reduce the problem to a singular integral equation in the Laplace transform domain. Itou [14] addressed the problem of two parallel interface cracks situated between a nonhomogeneous bonding layer and two dissimilar elastic half-planes subjected to an impact load. Despite these research efforts, the comprehension of the dynamic fracture behavior in nonhomogeneous coating-structure systems under impact loads remains relatively limited.

In recent years, the distributed dislocation technique (DDT) has been employed to solve more complex transient problems, including scenarios with multiple cracks, as outlined in references [15-17]. This method has demonstrated its superiority in terms of analytical simplicity and computational efficiency when compared to other approaches. Fallahnejad et al. [18] conducted research on the analytical solution for the impact loading involving Volterra-type screw dislocation in two functionally graded layers. In their study, they modeled the energy dissipation of FGM layers using viscous damping, and they assumed that the material properties change exponentially throughout the thickness of the layers. In the work of Bagheri [19], an analytical solution was explored for the case of anti-plane transient loading applied to two dissimilar orthotropic functionally graded half-layers with an interface containing a Volterra-type screw dislocation. This investigation employed linear elasticity theory as its foundation. The DSIFs were computed in the time domain using a combination of numerical Laplace inversion and the DDT. In their rigorous investigation, Bagheri and Monfared [20] explored the transient analysis of multiple cracks within a system consisting of two dissimilar half-planes under the influence of impactful loading. Their meticulous research provided profound insights into the intricate dynamics of this complex situation, making a significant contribution to the field of study.

To assess the necessity of repair or replacement for a structure featuring an interface crack within a material reinforced by FGM, the stress intensity factors acquired from a pertinent material investigation serve as a valuable resource. Leveraging the outcomes of this study mandates a careful comparison of dynamic stress intensity factors with the actual structural conditions. Should these factors surpass the permissible thresholds at critical junctures of the structure, the need for repair or replacement becomes evident. In this research, the transient response of an functionally graded coating and a homogeneous half-plane under mixed mode loading is thoroughly examined. The study employs the Distributed Dislocation Technique (DDT) and integral transforms, along with Stehfest's method [21]. Furthermore, the investigation delves into assessing the influence of various factors such as changes in material property gradients, Poisson's ratio, crack length, dimensionless time, coating thickness, and cracks interactions on transient SIFs. The insights gained from this study can be directly applied to inform the design of FG coating-substrate structures subjected to impact loads.

2 DISLOCATION SOLUTIONS

We consider an in-plane problem involving a homogeneous half-plane reinforced by a layer composed of FGM with a thickness denoted as *h*. Within this configuration, there exists a dislocation located at the interface, as illustrated in Figure 1. For our frame of reference, we adopt a Cartesian coordinate system where the x-axis is oriented to the right along the interface, and the y-axis extends upwards, aligned with the direction of the coating thickness.

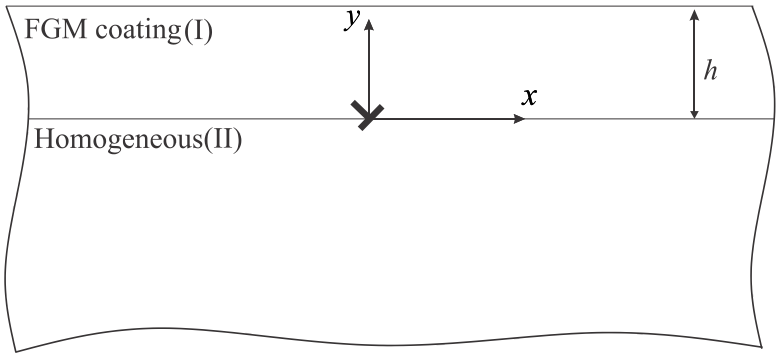

Fig. 1
Interface Dislocation between FGM Coating and Homogeneous Substrate.

In accordance with a well-established logical assumption, and with the aim of simplifying the solution of differential equations, a specialized coating composed of FGM is employed. In this FGM, the material constants vary in accordance with exponential laws. Consequently, the equations governing in-plane stresses in terms of elastic displacements within the FGM coating, in the absence of body forces, can be expressed as follows:

$$\sigma_{xx}(x,y,t)=\frac{\mu_0\exp(\beta y)}{\kappa-1}[(\kappa+1)\frac{\partial u}{\partial x}+(3-\kappa)\frac{\partial v}{\partial y}]$$

$$\sigma_{yy}(x,y,t)=\frac{\mu_0\exp(\beta y)}{\kappa-1}[(3-\kappa)\frac{\partial u}{\partial x}+(\kappa+1)\frac{\partial v}{\partial y}]$$

$$\tau_{xy}(x,y,t)=\mu_0\exp(\beta y)(\frac{\partial u}{\partial y}+\frac{\partial v}{\partial x}) \qquad 0\le y\le h \tag{1}$$

where:

- 'u' and 'v' denote the horizontal and vertical components of in-plane displacements, respectively.
- 'σ_{xx}','σ_{yy}' and 'τ_{xy}' describe components of the stress tensor.
- 'μ_0' signifies the elastic constant at the interface.
- 'β' denotes the FGM constant.
- '$\kappa=\begin{cases}(3-\upsilon)/(1+\upsilon) & plane\ \ stress\\ 3-4\upsilon & plane\ \ strain\end{cases}$' stands for the Kolosov constant.
- 'υ' denotes the Poisson ratio of the material.

By substituting the stress components as expressed in equations (1) into the equations of motion, the equations governing the behavior of the FGM coating can be reformulated as follows:

$$(\kappa+1)\frac{\partial^2 u}{\partial x^2}+2\frac{\partial^2 v}{\partial x\partial y}+(\kappa-1)\frac{\partial^2 u}{\partial y^2}+\beta(\kappa-1)(\frac{\partial u}{\partial y}+\frac{\partial v}{\partial x})=c^2(\kappa-1)\frac{\partial^2 u}{\partial t^2}$$

$$(\kappa-1)\frac{\partial^2 v}{\partial x^2}+2\frac{\partial^2 u}{\partial x\partial y}+(\kappa+1)\frac{\partial^2 v}{\partial y^2}+\beta(\kappa+1)\frac{\partial v}{\partial y}+\beta(3-\kappa)\frac{\partial u}{\partial x}=c^2(\kappa-1)\frac{\partial^2 v}{\partial t^2} \qquad 0\le y\le h \tag{2}$$

The mass density within the FGM coating, similar to the elastic modulus, is described exponentially:

$$\rho(y)=\rho_0\exp(\beta y) \tag{3}$$

where ρ_0 denotes the material density at $y=0$, while $1/c=\sqrt{\mu_0/\rho_0}$ represents the shear wave velocity of the material. In Equations (2), when setting $\beta=0$, the equations of motion for a homogeneous half-plane $y\le 0$ are derived as follows:

$$(\kappa+1)\frac{\partial^2 u}{\partial x^2}+2\frac{\partial^2 v}{\partial x\partial y}+(\kappa-1)\frac{\partial^2 u}{\partial y^2}=c^2(\kappa-1)\frac{\partial^2 u}{\partial t^2}$$

$$(\kappa-1)\frac{\partial^2 v}{\partial x^2}+2\frac{\partial^2 u}{\partial x\partial y}+(\kappa+1)\frac{\partial^2 v}{\partial y^2}=c^2(\kappa-1)\frac{\partial^2 v}{\partial t^2} \qquad y\le 0 \tag{4}$$

With reference to Figure 1, the traction-free conditions, in conjunction with equations describing the continuity requirements specific to the medium in question, can be formulated as follows:

$$\sigma_{yy}(x,h,t)=0$$

$$\tau_{xy}(x,h,t)=0$$

$$\begin{bmatrix}u(x,0^+,t)\\ v(x,0^+,t)\end{bmatrix}-\begin{bmatrix}u(x,0^-,t)\\ v(x,0^-,t)\end{bmatrix}=\begin{bmatrix}b_x(t)\\ b_y(t)\end{bmatrix}H(x)$$

$$\sigma_{yy}(x,0^+,t)=\sigma_{yy}(x,0^-,t)$$

$$\tau_{xy}(x,0^+,t)=\tau_{xy}(x,0^-,t) \tag{5}$$

Here, $H(.)$ represents the Heaviside step function. The glide and climb of edge dislocations situated at the center of the coordinate system, represented by $b_x(t)$ and $b_y(t)$, are along the $y=0$ axis and in the positive x direction. To achieve the desired stress fields, it is expedient to begin with the assumption that the system is in a state of rest. Consequently, by employing Laplace and Fourier transforms on equations (2) and (4) with respect to the time variable (t) and spatial variable (x), respectively, while considering the stress components in the far field as negligible, the subsequent outcomes can be derived:

$$\begin{cases}(\kappa-1)\dfrac{d^2U^*}{dy^2}+\beta(\kappa-1)\dfrac{dU^*}{dy}+2i\zeta\dfrac{dV^*}{dy}+i\zeta\beta(\kappa-1)V^*-[\zeta^2(\kappa+1)+c^2(\kappa-1)s^2]U^*=0\\ (\kappa+1)\dfrac{d^2V^*}{dy^2}+\beta(\kappa+1)\dfrac{dV^*}{dy}+2i\zeta\dfrac{dU^*}{dy}+i\zeta\beta(3-\kappa)U^*-[\zeta^2(\kappa-1)+c^2(\kappa-1)s^2]V^*=0\end{cases} \quad 0\le y\le h \tag{6a}$$

$$\begin{cases}(\kappa-1)\dfrac{d^2U^*}{dy^2}+2i\zeta\dfrac{dV^*}{dy}-[\zeta^2(\kappa+1)+c^2(\kappa-1)s^2]U^*=0\\ (\kappa+1)\dfrac{d^2V^*}{dy^2}+2i\zeta\dfrac{dU^*}{dy}-[\zeta^2(\kappa-1)+c^2(\kappa-1)s^2]V^*=0\end{cases} \quad y\le 0 \tag{6b}$$

The Laplace transform is denoted by the symbol $*$. The Laplace parameter is 's', the imaginary unit is '$i=\sqrt{-1}$', and the Fourier parameter is 'ζ'. The Fourier transforms of the displacement components 'u' and 'v' are denoted by 'U' and 'V', respectively. The answer to the problem in both regions, $y\le 0$ and $0\le y\le h$, can be derived as follows:

$$\begin{cases}U^*(\zeta,y,s)=C_1e^{r_1y}+C_2e^{r_2y}+C_3e^{r_3y}+C_4e^{r_4y}\\ V^*(\zeta,y,s)=ib_{11}C_1e^{r_1y}+ib_{21}C_2e^{r_2y}+ib_{31}C_3e^{r_3y}+ib_{41}C_4e^{r_4y}\end{cases} \quad y\le 0 \tag{7a}$$

$$\begin{cases}U^*(\zeta,y,s)=A_1e^{\lambda_1y}+A_2e^{\lambda_2y}+A_3e^{\lambda_3y}+A_4e^{\lambda_4y}\\ V^*(\zeta,y,s)=ia_{11}A_1e^{\lambda_1y}+ia_{21}A_2e^{\lambda_2y}+ia_{31}A_3e^{\lambda_3y}+ia_{41}A_4e^{\lambda_4y}\end{cases} \quad 0\le y\le h \tag{7b}$$

Given that the $\{A_m,C_m\},m=1,2,3,4$ represents the functions to be determined, we are given the eigenvalues $\{\lambda_m,r_m\},m=1,2,3,4$ and the functions $\{a_{m1},b_{m1}\},m=1,2,3,4$ as follows:

$$\begin{cases}r_1=\sqrt{\zeta^2+c^2s^2},r_2=\sqrt{\zeta^2+c^2s^2\dfrac{\kappa-1}{\kappa+1}}, \quad \mathrm{Re}(r_1,r_2)>0\\ r_3=-\sqrt{\zeta^2+c^2s^2},r_4=-\sqrt{\zeta^2+c^2s^2\dfrac{\kappa-1}{\kappa+1}}, \quad \mathrm{Re}(r_3,r_4)<0 \quad y\le 0\\ b_{j1}=\dfrac{(\kappa-1)r_j^2-[\zeta^2(\kappa+1)+c^2(\kappa-1)s^2]}{2\zeta r_j}, \quad j=1,2,3,4\end{cases} \tag{8a}$$

$$\begin{cases}\lambda_1=\dfrac{1}{2}[-\beta-\sqrt{\beta^2-2\Delta_3+2\sqrt{\Delta_3^2-4\Delta_4}}],\lambda_2=\dfrac{1}{2}[-\beta-\sqrt{\beta^2-2\Delta_3-2\sqrt{\Delta_3^2-4\Delta_4}}], \quad \mathrm{Re}(\lambda_1,\lambda_2)<0\\ \lambda_3=\dfrac{1}{2}[-\beta+\sqrt{\beta^2-2\Delta_3+2\sqrt{\Delta_3^2-4\Delta_4}}],\lambda_4=\dfrac{1}{2}[-\beta+\sqrt{\beta^2-2\Delta_3-2\sqrt{\Delta_3^2-4\Delta_4}}], \quad \mathrm{Re}(\lambda_3,\lambda_4)>0 \quad 0\le y\le h\\ a_{j1}=\dfrac{(\kappa-1)\lambda_j^2+\beta(\kappa-1)\lambda_j-[\zeta^2(\kappa+1)+c^2(\kappa-1)s^2]}{\zeta[2\lambda_j+\beta(\kappa-1)]}, \quad j=1,2,3,4\end{cases} \tag{8b}$$

In the equations presented above, the newly introduced variable is precisely defined as follows:

$$\Delta_3 = -2\zeta^2 - \frac{2c^2\kappa s^2}{\kappa+1}$$

$$\Delta_4 = \zeta^4 + \frac{2c^2\kappa s^2\zeta^2}{\kappa+1} + \frac{c^4 s^4(\kappa-1)}{\kappa+1} - \zeta^2\beta^2\frac{\kappa-3}{\kappa+1} \tag{9}$$

Given that the displacements in equations (7a) must exhibit bounded behavior as y approaches $-\infty$, the coefficients C_3 and C_4 converge to zero. The inverse transform of the displacements in equations (7a) and (7b) yields the subsequent outcomes:

$$\begin{cases} u^*(x,y,s) = \dfrac{1}{2\pi}\displaystyle\int_{-\infty}^{\infty}(C_1 e^{r_1 y} + C_2 e^{r_2 y})e^{i\zeta x}d\zeta \\ v^*(x,y,s) = \dfrac{i}{2\pi}\displaystyle\int_{-\infty}^{\infty}(b_{11}C_1 e^{r_1 y} + b_{21}C_2 e^{r_2 y})e^{i\zeta x}d\zeta \end{cases} \qquad y \le 0 \tag{10a}$$

$$\begin{cases} u^*(x,y,s) = \dfrac{1}{2\pi}\displaystyle\int_{-\infty}^{\infty}(A_1 e^{\lambda_1 y} + A_2 e^{\lambda_2 y} + A_3 e^{\lambda_3 y} + A_4 e^{\lambda_4 y})e^{i\zeta x}d\zeta \\ v^*(x,y,s) = \dfrac{i}{2\pi}\displaystyle\int_{-\infty}^{\infty}(a_{11}A_1 e^{\lambda_1 y} + a_{21}A_2 e^{\lambda_2 y} + a_{31}A_3 e^{\lambda_3 y} + a_{41}A_4 e^{\lambda_4 y})e^{i\zeta x}d\zeta \end{cases} \qquad 0 \le y \le h \tag{10b}$$

Ultimately, by utilizing equations (1), (10a), and (10b), the stress components in the Laplace-transformed space of the regions under investigation can be precisely formulated as shown below:

$$\begin{cases} \sigma_{xx}^*(x,y,s) = \dfrac{i\mu_0}{2\pi(\kappa-1)}\displaystyle\int_{-\infty}^{\infty}(b_{12}C_1 e^{r_3 y} + b_{22}C_2 e^{r_4 y})e^{i\zeta x}d\zeta \\ \sigma_{yy}^*(x,y,s) = \dfrac{i\mu_0}{2\pi(\kappa-1)}\displaystyle\int_{-\infty}^{\infty}(b_{13}C_1 e^{r_3 y} + b_{23}C_2 e^{r_4 y})e^{i\zeta x}d\zeta \\ \tau_{xy}^*(x,y,s) = \dfrac{\mu_0}{2\pi}\displaystyle\int_{-\infty}^{\infty}(b_{14}C_1 e^{r_3 y} + b_{24}C_2 e^{r_4 y})e^{i\zeta x}d\zeta \end{cases} \qquad y \le 0 \tag{11a}$$

$$\begin{cases} \sigma_{xx}^*(x,y,s) = \dfrac{i\mu_0 e^{\beta y}}{2\pi(\kappa-1)}\displaystyle\int_{-\infty}^{\infty}(a_{12}A_1 e^{\lambda_1 y} + a_{22}A_2 e^{\lambda_2 y} + a_{32}A_3 e^{\lambda_3 y} + a_{42}A_4 e^{\lambda_4 y})e^{i\zeta x}d\zeta \\ \sigma_{yy}^*(x,y,s) = \dfrac{i\mu_0 e^{\beta y}}{2\pi(\kappa-1)}\displaystyle\int_{-\infty}^{\infty}(a_{13}A_1 e^{\lambda_1 y} + a_{23}A_2 e^{\lambda_2 y} + a_{33}A_3 e^{\lambda_3 y} + a_{43}A_4 e^{\lambda_4 y})e^{i\zeta x}d\zeta \\ \tau_{xy}^*(x,y,s) = \dfrac{\mu_0 e^{\beta y}}{2\pi}\displaystyle\int_{-\infty}^{\infty}(a_{14}A_1 e^{\lambda_1 y} + a_{24}A_2 e^{\lambda_2 y} + a_{34}A_3 e^{\lambda_3 y} + a_{44}A_4 e^{\lambda_4 y})e^{i\zeta x}d\zeta \end{cases} \qquad 0 \le y \le h \tag{11b}$$

where, the functions $\{b_{j2}, b_{j3}, b_{j4}\}$, $j = 1,2$ and $\{a_{j2}, a_{j3}, a_{j4}\}$, $j = 1,2,3,4$ are specified as follows:

$$\begin{cases} b_{j2} = (\kappa+1)\zeta + (3-\kappa)b_{j1}r_j \\ b_{j3} = (3-\kappa)\zeta + (\kappa+1)b_{j1}r_j \quad j=1,2 \\ b_{j4} = r_j - \zeta b_{j1} \end{cases}$$

$$\begin{cases} a_{j2} = (\kappa+1)\zeta + (3-\kappa)a_{j1}\lambda_j \\ a_{j3} = (3-\kappa)\zeta + (\kappa+1)a_{j1}\lambda_j \quad j=1,2,3,4 \\ a_{j4} = \lambda_j - \zeta a_{j1} \end{cases} \tag{12}$$

By analyzing the boundary conditions (5) using Fourier and Laplace transforms, and utilizing the expressions from equations (7a-7b) and (11a-11b), the unknown coefficients ($A_m, m=1,2,3,4$ and $C_m, m=1,2$) can be rigorously determined as follows:

$$C_j = [C_{j1}b_x(s) + iC_{j2}b_y(s)](\pi\delta(\zeta) - i/\zeta), \quad j=1,2 \tag{13a}$$

$$A_j = [A_{j1}b_x(s) + iA_{j2}b_y(s)](\pi\delta(\zeta) - i/\zeta), \quad j=1,2,3,4 \tag{13b}$$

where $\delta(.)$ represents the Dirac delta function. Following a series of systematic manipulations, the undetermined functions $C_{j1}, C_{j2}, j \in \{1,2\}$, and $A_{j1}, A_{j2}, j \in \{1,2,3,4\}$ in Eqs. (13a) and (13b), defined in Appendix I, can be derived. The stress fields in the $y \le 0$ can subsequently be obtained utilizing Eqs. (11a) and (13a) as follows:

$$\begin{cases} \sigma^*_{xx}(x,y,s) = \dfrac{\mu_0}{2\pi(\kappa-1)} \displaystyle\int_{-\infty}^{\infty} \frac{e^{i\zeta x}}{\zeta} [(b_{12}C_{11}e^{r_1 y} + b_{22}C_{21}e^{r_2 y})b_x(s) + i(b_{12}C_{12}e^{r_1 y} + b_{22}C_{22}e^{r_2 y})b_y(s)]d\zeta \\ \sigma^*_{yy}(x,y,s) = \dfrac{\mu_0}{2\pi(\kappa-1)} \displaystyle\int_{-\infty}^{\infty} \frac{e^{i\zeta x}}{\zeta} [(b_{13}C_{11}e^{r_1 y} + b_{23}C_{21}e^{r_2 y})b_x(s) + i(b_{13}C_{12}e^{r_1 y} + b_{23}C_{22}e^{r_2 y})b_y(s)]d\zeta \quad y \le 0 \\ \tau^*_{xy}(x,y,s) = \dfrac{\mu_0}{2\pi} \displaystyle\int_{-\infty}^{\infty} \frac{-ie^{i\zeta x}}{\zeta} [(b_{14}C_{11}e^{r_1 y} + b_{24}C_{21}e^{r_2 y})b_x(s) + i(b_{14}C_{12}e^{r_1 y} + b_{24}C_{22}e^{r_2 y})b_y(s)]d\zeta \end{cases} \tag{14}$$

In order to conduct a numerical computation of the stress field components, the integrals as presented in equations (14) can be partitioned into both odd and even segments and reformulated in the following equation format:

$$\sigma^*_{mn}(x,y,s) = \int_0^{\infty} F_{mn}(x,y,s,\zeta)d\zeta, \quad m,n \in \{x,y\} \tag{15}$$

where the functions $g_{mn}(x,y,s,\zeta), m,n \in \{x,y\}$ are defined as follows:

$$F_{xx}(x,y,s,\xi) = \frac{\mu_0}{\pi(\kappa-1)\xi}[(b_{12}C_{11}e^{r_1 y} + b_{22}C_{21}e^{r_2 y})b_x(s)\cos(\xi x) - (b_{12}C_{12}e^{r_1 y} + b_{22}C_{22}e^{r_2 y})b_y(s)\sin(\xi x)]$$

$$F_{yy}(x,y,s,\xi) = \frac{\mu_0}{\pi(\kappa-1)\xi}[(b_{13}C_{11}e^{r_1 y} + b_{23}C_{21}e^{r_2 y})b_x(s)\cos(\xi x) - (b_{13}C_{12}e^{r_1 y} + b_{23}C_{22}e^{r_2 y})b_y(s)\sin(\xi x)]$$

$$F_{xy}(x,y,s,\xi) = \frac{\mu_0}{\pi\xi}[(b_{14}C_{11}e^{r_1 y} + b_{24}C_{21}e^{r_2 y})b_x(s)\sin(\xi x) + (b_{14}C_{12}e^{r_1 y} + b_{24}C_{22}e^{r_2 y})b_y(s)\cos(\xi x)] \tag{16}$$

Observing equation (16), it becomes evident that the integrals in equation (15) become infinite for adjacent dislocation points, rendering the calculation impractical and preventing the attainment of exact results. To address this challenge, we examine the singularity of the kernels F_{mn} through their limit values, denoted as $\zeta \to \infty$, as follows:

$$F_{mn}(x,y,s,\zeta) = \underbrace{F_{mn\infty}(x,y,s,\zeta)}_{Singular\ Part} + \underbrace{[F_{mn}(x,y,s,\zeta) - F_{mn\infty}(x,y,s,\zeta)]}_{Non\sin gular\ Part},\ \ m,n \in \{x,y\}. \tag{17}$$

As ζ tends towards infinity, we utilize the subsequent relationships to compute the asymptotic values of the F_{ij} kernels in equations (16).

$$\begin{bmatrix} F_{xx\infty}(x,y,s,\zeta) \\ F_{yy\infty}(x,y,s,\zeta) \\ F_{xy\infty}(x,y,s,\zeta) \end{bmatrix} = \frac{2\mu_0 e^{-\zeta y}}{\pi(\kappa+1)} \{ \begin{bmatrix} (2-\zeta y)\cos(\zeta x) \\ \zeta y \cos(\zeta x) \\ (\zeta y - 1)\sin(\zeta x) \end{bmatrix} b_x(s) + \begin{bmatrix} (\zeta y - 1)\sin(\zeta x) \\ (-\zeta y - 1)\sin(\zeta x) \\ \zeta y \cos(\zeta x) \end{bmatrix} b_y(s) \}, \tag{18}$$

Through algebraic manipulations, equation (15), when considered in light of equations (17) and (18), can be restructured into a more convenient form as follows:

$$\sigma^*_{xx}(x,y,s) = \frac{2\mu_0}{\pi(\kappa+1)} \frac{y(3x^2+y^2)b_x(s) + x(y^2-x^2)b_y(s)}{(x^2+y^2)^2} + \int_0^\infty [F_{xx}(x,y,s,\zeta) - F_{xx\infty}(x,y,s,\zeta)]d\zeta,$$

$$\sigma^*_{yy}(x,y,s) = \frac{2\mu_0}{\pi(\kappa+1)} \frac{y(y^2-x^2)b_x(s) - x(x^2+3y^2)b_y(s)}{(x^2+y^2)^2} + \int_0^\infty [F_{yy}(x,y,s,\zeta) - F_{yy\infty}(x,y,s,\zeta)]d\zeta,$$

$$\tau^*_{xy}(x,y,s) = \frac{2\mu_0}{\pi(\kappa+1)} \frac{x(y^2-x^2)b_x(s) - y(y^2-x^2)b_y(s)}{(x^2+y^2)^2} + \int_0^\infty [F_{xy}(x,y,s,\zeta) - F_{xy\infty}(x,y,s,\zeta)]d\zeta, \tag{19}$$

The relationships presented in equation (19) exhibit bounded behavior and converge rapidly, particularly for large values of 'ζ', rendering the integrals amenable to numerical evaluation.

3 MULTIPLE INTERFACE CRACKS FORMULATION

The integral equations for the given problem can be derived through the utilization of the dislocation solution as Green's function. Consequently, the dislocation solution can be employed to analyze the aforementioned structure with cracks when subjected to impact loads. The geometry of the crack can be parametrically described as follows:

$$\begin{aligned} &x_m(\alpha) = x_{0m} + \alpha l_m, \\ &y_m(\alpha) = 0, \qquad -1 \le \alpha \le 1, \quad m \in \{1,2,3,...,N\} \end{aligned} \tag{20}$$

where $(x_{0m}, 0)$ and l_m represent the center and half-length of the crack, respectively. Applying the principle of superposition to stress components at the point (x_i, y_i) on the boundary of the *i*-th crack, where the parameter $-1 \le \alpha \le 1$, yields the following relationships:

$$\begin{bmatrix}\sigma^*_{yy}(x_m(\alpha),y_m(\alpha),s)\\ \sigma^*_{xy}(x_m(\alpha),y_m(\alpha),s)\end{bmatrix}=\sum_{k=1}^{N}l_k\int_{-1}^{1}[\begin{bmatrix}k^{11}_{yymk}(\alpha,\beta,s)\\ k^{11}_{xymk}(\alpha,\beta,s)\end{bmatrix}b_{xk}(\beta,s)+\begin{bmatrix}k^{12}_{yymk}(\alpha,\beta,s)\\ k^{12}_{xymk}(\alpha,\beta,s)\end{bmatrix}b_{yk}(\beta,s)]d\beta, \quad m=1,2,...,N,-1\le\alpha\le 1. \tag{21}$$

In these equations, $b_{xk}(\beta,s)$ and $b_{yk}(\beta,s)$ are the Laplace-transformed dislocation densities at the *k*-th crack. The coefficients $k^{1n}_{lm},n=1,2,l,m=x,y$ are coefficients of $b_x(s)$ and $b_y(s)$ in equations (19). The kernels in equations (21) exhibit the singularity of the Cauchy form for $i=k$ as $q\to p$, and are expressed as follows:

$$k^{1z}_{wyii}(\alpha,\beta,s)=-\frac{2\mu_0}{\pi l_i(\kappa+1)(\alpha-\beta)}+\sum_{m=0}^{\infty}a_{1z,mi}(\beta,s)(\alpha-\beta)^m \qquad z\in\{1,2\},w\in\{x,y\} \tag{22}$$

The singularity of the equation is derived by the leading terms of the Taylor series expansion of $x_i(\beta)$ and $y_i(\beta)$ about β. As per Bueckner's theorem [22] of superposition, the expression on the left of equations (21), with opposite signs, represents the traction induced by the external load acting on the assumed crack surfaces between the two materials. The integral equations (21) must be solved subject to the following single-valued conditions:

$$\int_{-1}^{1}b_{ri}(\beta,s)d\beta=0,\ \ r\in\{x,y\},\ \ i\in\{1,2,...,N\} \tag{23}$$

It can be demonstrated that the kernel of integral equations (21) exhibits a Cauchy-type singularity exclusively. Consequently, the dislocation density is considered as follows:

$$b_{ri}(\beta,s)=\frac{g_{ri}(\beta,s)}{\sqrt{1-\beta^2}},\ \ r\in\{x,y\},\ \ -1<\beta<1,\ \ \ i\in\{1,2,...,N\} \tag{24}$$

The unknown functions $g_{ki}(\beta,s)$ are bounded. By substituting Eq. (24) into equations (21) and (23) and utilizing the Lobatto–Chebyshev integration formula, the discretized singular integral equations are obtained as follows:

$$\int_{-1}^{1}k^{1h}_{myij}(\alpha,\beta,s)\frac{g_{ij}(\beta,s)}{\sqrt{1-\beta^2}}d\beta=\frac{\pi}{n-1}\sum_{r=1}^{n}e_r k^{1h}_{myij}(\alpha_d,\beta_r,s)g_{ij}(\beta_r,s),\quad m\in\{x,y\},\ h\in\{1,2\} \tag{25}$$

where the $\beta_r=\cos[\frac{(r-1)\pi}{n-1}],\ r\in\{1,2,...,n\}$, $\alpha_d=\cos[\frac{(2d-1)\pi}{2(n-1)}],\ d\in\{1,2,...,n-1\}$, $e_r=0.5$ for $r=1,n$, and $e_r=1$ for $1<r<n$. Baghestani et al. [23] define modes I and II DSIFs at embedded crack tips as follows:

$$K^*_I(s)=\lim_{r\to 0}\sqrt{2r}\sigma^*_{yy}(r,\theta,s),\ \ K^*_{II}(s)=\lim_{r\to 0}\sqrt{2r}\sigma^*_{xy}(r,\theta,s). \tag{26}$$

where r represents the proximity to the crack tip, and $\theta=0$ for the right crack tip and $\theta=\pi$ for the left crack tip, respectively. By incorporating equations (22) and (24) into equations (21) and utilizing the outcome in equations (26), the DSIFs at the *i*-th crack tip are expressed by dislocation densities as follows:

$$K^*_{Ii}(s)=-\frac{2\mu_0\eta}{\kappa+1}\sqrt{l_i}g_{yi}(\eta,s),$$

$$K_{IIi}^{*}(s)=-\frac{2\mu_0\eta}{\kappa+1}\sqrt{l_i}\,g_{xi}(\eta,s),\ \ i\in\{1,2,...,N\}. \tag{27}$$

where $\eta=1$ represents the right crack tip, and $\eta=-1$ corresponds to the left crack tip. To keep the text concise, the detailed derivation of DIFs is not provided here. The inverse Laplace transform of DSIFs is computed numerically using Stehfest's method.

4 FINDING AND INTERPRETATION

This portion of the research is divided into two primary divisions. The first section focuses on verifying the obtained solutions, while the second part entails solving new examples to illustrate the procedure's applicability. In the calculation procedure, we examine a homogeneous half-plane reinforced by an FG coating under plane strain conditions, with material properties as provided below:

Table. 1
The mechanical properties of the medium

Poisson's ratio	modulus of elasticity	mass density
$\upsilon=0.3$	$E_0=200GPa$	$\rho_0=7840\,kg/m^3$

In the calculations for the inverse Laplace transforms, M is set to 10. Interestingly, $K_0=\sigma_0\sqrt{l}$ and $K_0=\tau_0\sqrt{l}$ calibrate the DSIFs for normal and shear loading regimes. Notably, l marks the crack's half-length, and K_0 signifies the static SIF value for a single crack within a homogeneous plane under static traction. Herein, K_I and K_{II} assume the roles of DSIF identifiers for fracture mechanics modes I and II, respectively.

The initial reliability of this study is assessed by examining a crack in an infinite plane, with $\beta=0$ and $h\to\infty$. Uniformly distributed normal loads are applied along the crack. The variations of normalized DSIFs for a crack are illustrated in Figure 2, where $t_0=l\sqrt{\rho_0/\mu_0}$. Figure 2 clearly demonstrated the close agreement between this study and the findings of Sih et al. [24] and Mottale et al. [25].

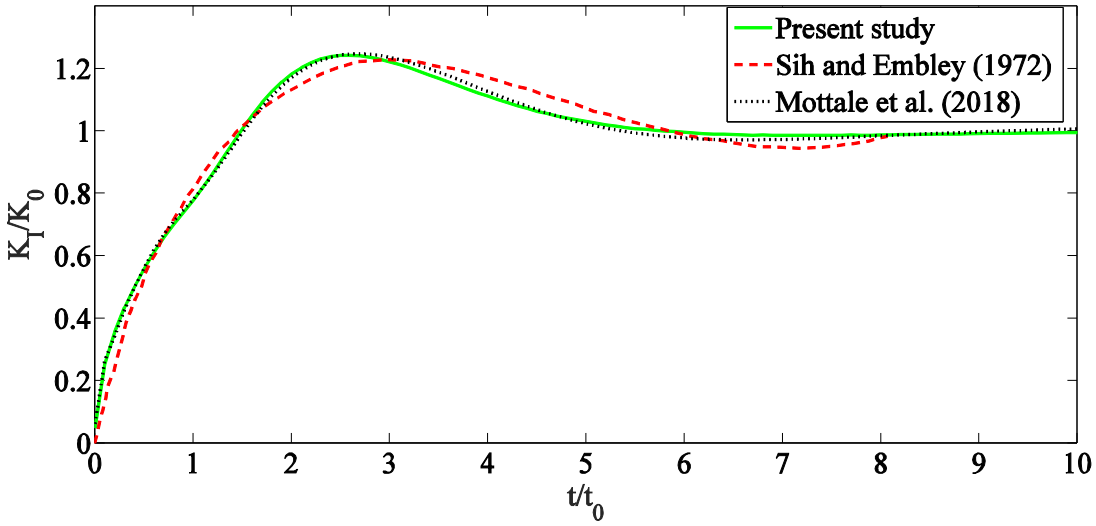

Fig. 2
A comparison of the DSIFs for a crack in an infinite plane versus t/t_0 .

To further validate our analysis, we consider two dissimilar half-planes, one elastic and one functionally graded (FG), containing a crack under normal loading. In this case, we let $h \to \infty$ and $\beta l = 0.5,1.0$, $2l = 2cm$. This configuration allows us to directly compare our results with the well-established solution presented by Jafari et al. [26]. As depicted in Figure 3, our results achieve excellent agreement with the reference solution.

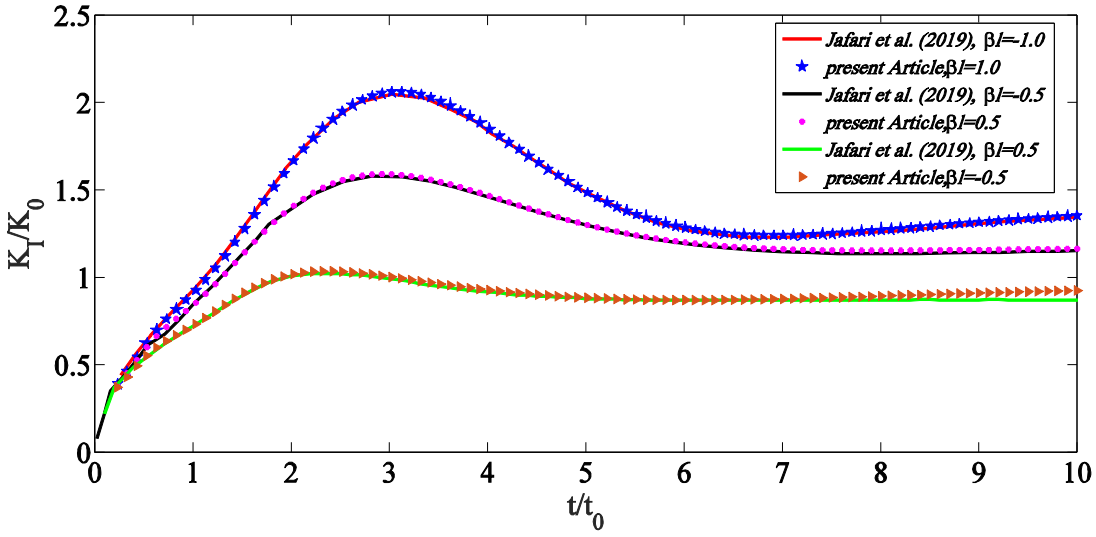

Fig. 3
Comparison of DSIFs at crack tips in nonhomogeneous and homogeneous half-planes: Validation of a numerical model.

In Figures 4 to 13, we investigate a homogeneous half-plane reinforced by an FG coating with $\beta = 2.5,5.0\,cm^{-1}$ and including a $2l = 0.2,0.4cm$ interfacial crack. The structure is subjected to uniform normal, shear and mixed mode loading.

The normalized transient DSIFs for modes I and II, considering various nonhomogeneous parameters ($\beta = 2.5,5.0\,cm^{-1}$) and crack lengths ($2l = 0.2,0.4cm$), are depicted in Figs. 4 and 5 for normal traction. These figures exhibit a common trend where the DSIF values rapidly increase with time, reach a peak, and subsequently oscillate around the corresponding static value. For mode I, the DSIFs at the left and right crack tips are identical due to the problem's symmetry under normal loading. However, in mode II, the DSIFs at the left and right crack tips differ and have opposite signs. The symmetry of the problem for mode I and anti-symmetry for mode II under normal loading are the reasons for the observed behavior, as reported in Tables 2 and 4 of [27]. Indeed, both the peak and steady-state values of DSIFs decrease with an increasing FG exponent β. This is a result of the material gradient parameter causing the coating to become stiffer than the homogeneous half-plane substrate. As expected, the DSIFs exhibit mixed-mode behavior, even when the loading is of a single mode, due to the heterogeneity of the medium under investigation. Additionally, it is observed that the DSIFs increase with an increase in the crack length l.

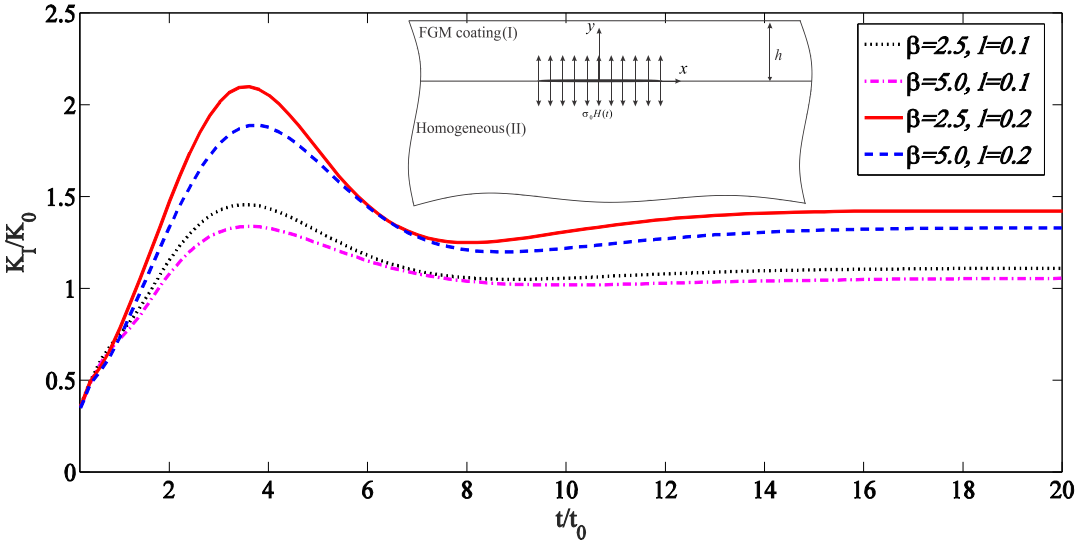

Fig. 4 Mode-I fracture behavior of an interface crack in nonhomogeneous media under normal loading.

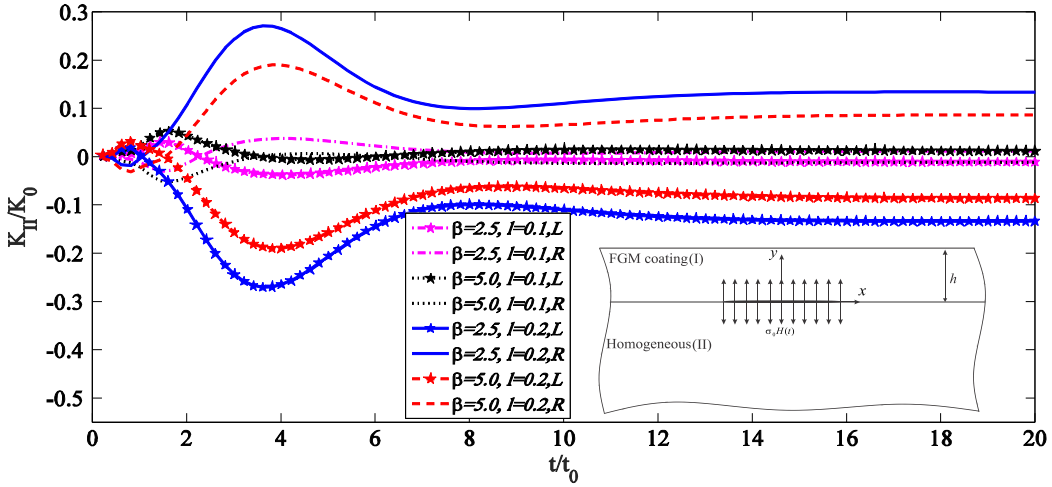

Fig. 5
Mode-II DSIFs of an interface under normal loading.

Fig. 6 provides a comprehensive visualization of the magnitude of normalized DSIFs under mixed mode loading conditions. These factors pertain to a situation where a crack is positioned at the interface between two distinct mediums. The temporal evolution of these DSIFs closely follows the trends observed in the preceding examples.

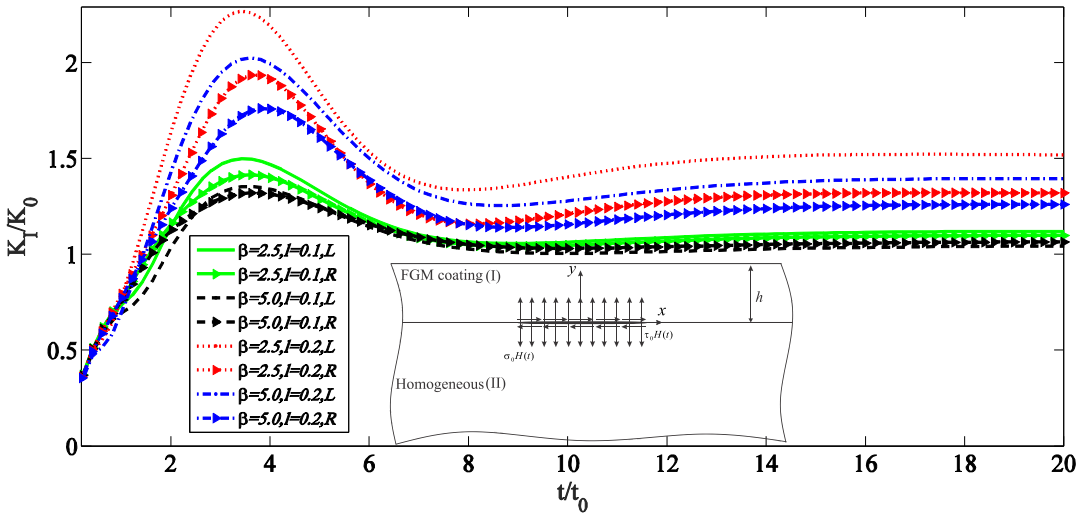

Fig. 6 Mode-I DSIFs: Sensitive to nonhomogeneity, crack length, and mixed-mode loading.

Figs. (7-9) present the variations of dimensionless modes I and II DSIFs with respect to t/t_0 for different nonhomogeneous parameters $\beta = 2.5,5.0cm^{-1}$ and the thickness of the coating $h/l = 1.0,2.0$ in the case of an interface crack subjected to normal, shear, and mixed mode loading conditions. In these instances, the DSIFs rapidly increase from zero to a peak value significantly above their corresponding static values and then oscillate around them. Notably, it can be observed that the DSIFs for $h/l = 1.0$ are higher than those for $h/l = 2.0$. Furthermore, the influence of the nonhomogeneous parameters of the FG coating on the DSIFs is clearly demonstrated.

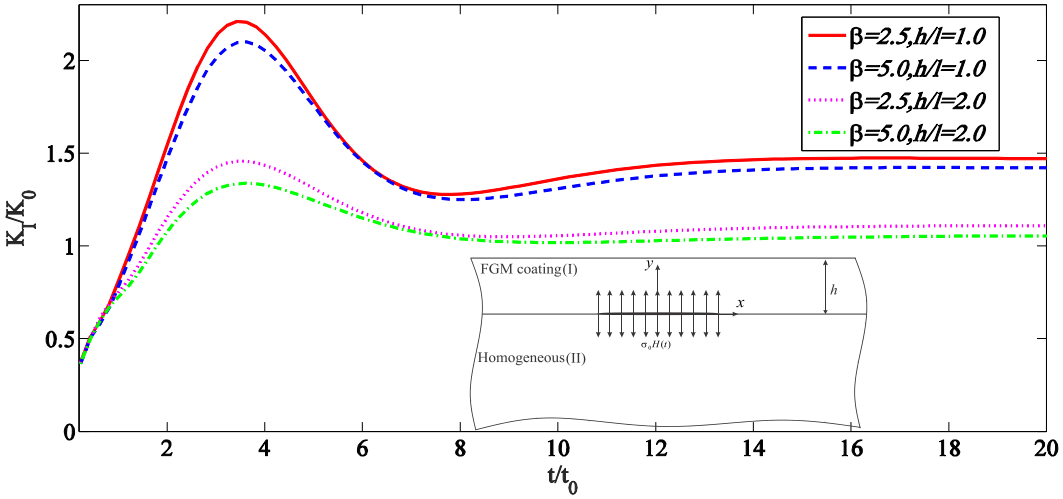

Fig. 7
Transient mode-I DSIFs of an interface crack under normal loading: effects of nonhomogeneity and coating thickness.

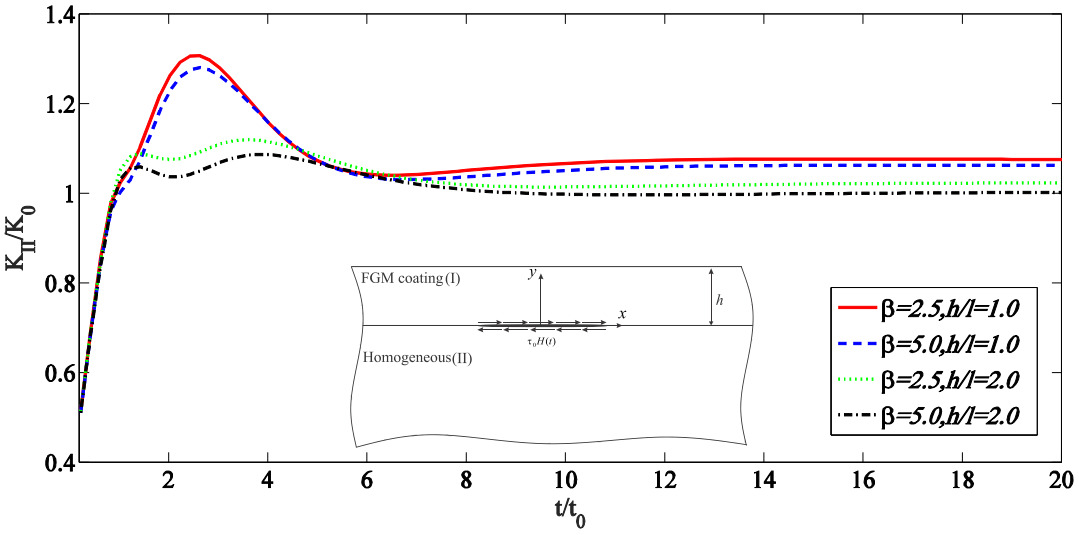

Fig. 8
Transient DSIFs of an interface crack: a study of nonhomogeneity and coating thickness.

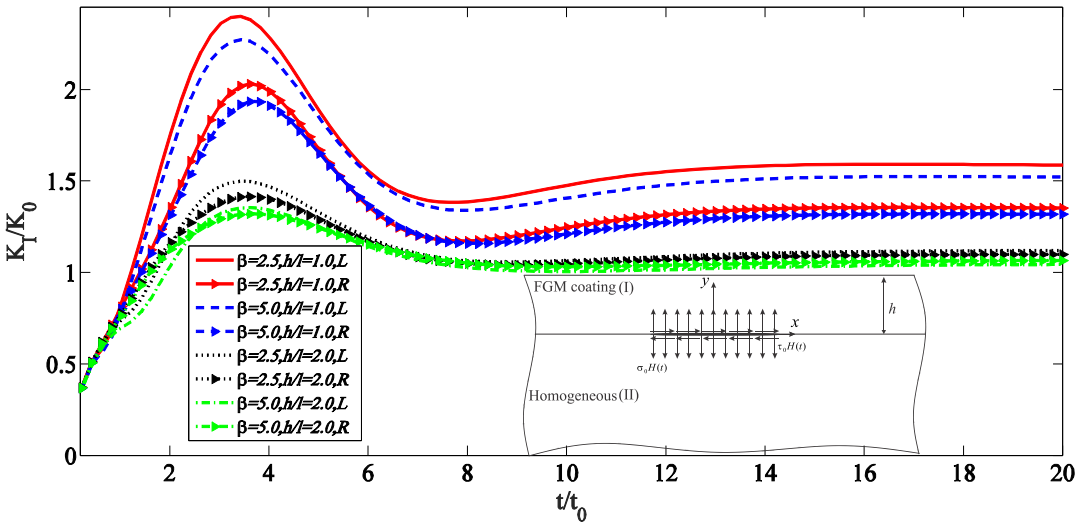

Fig. 9
The role of nonhomogeneity and coating thickness in the mixed mode loading behavior of an interface crack on the mode I DSIFs.

The graphical representations in Figs. 10 to 13 illustrate the impacts of coating thickness and Poisson's ratio on non-dimensional DSIFs for normal, shear, and mixed-mode loading. In these graphs, the nonhomogeneous parameter is set at $\beta = 5cm^{-1}$, and the crack length is $2l = 2cm^{-1}$. It becomes evident that as the coating thickness increases, the normalized DSIFs exhibit a decrease. Additionally, with an increase in Poisson's ratio, the maximum value of DSIFs is reached in a shorter time. In addition, the effect of Poisson's ratio variation on the maximum value of DSIFs is insignificant.

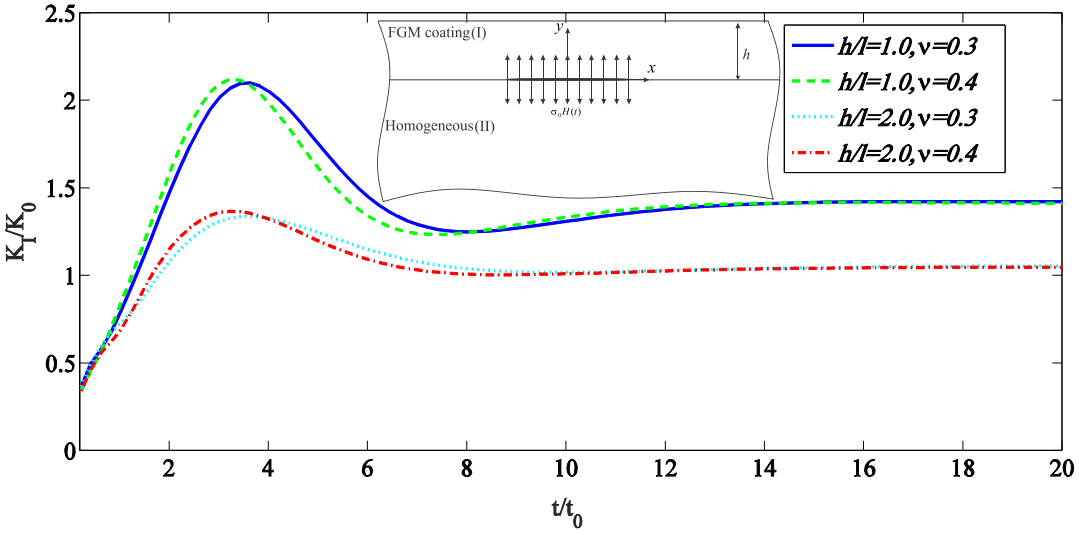

Fig. 10
Transient mode-I DSIFs of an interface crack under normal loading: effects of Poisson's ratio and coating thickness.

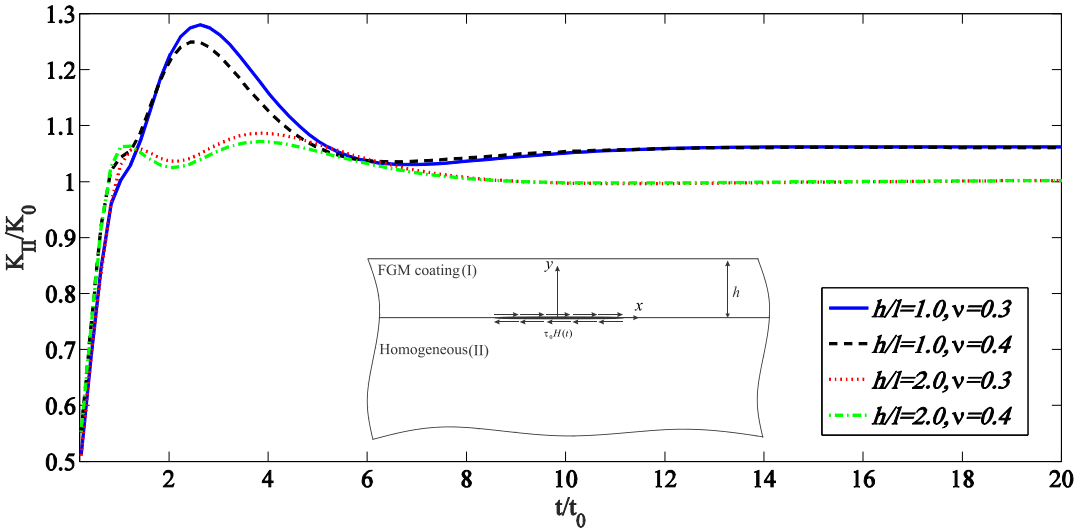

Fig. 11
Transient mode II DSIFs of an interface crack under shear loading: a study of Poisson's ratios and coating thickness.

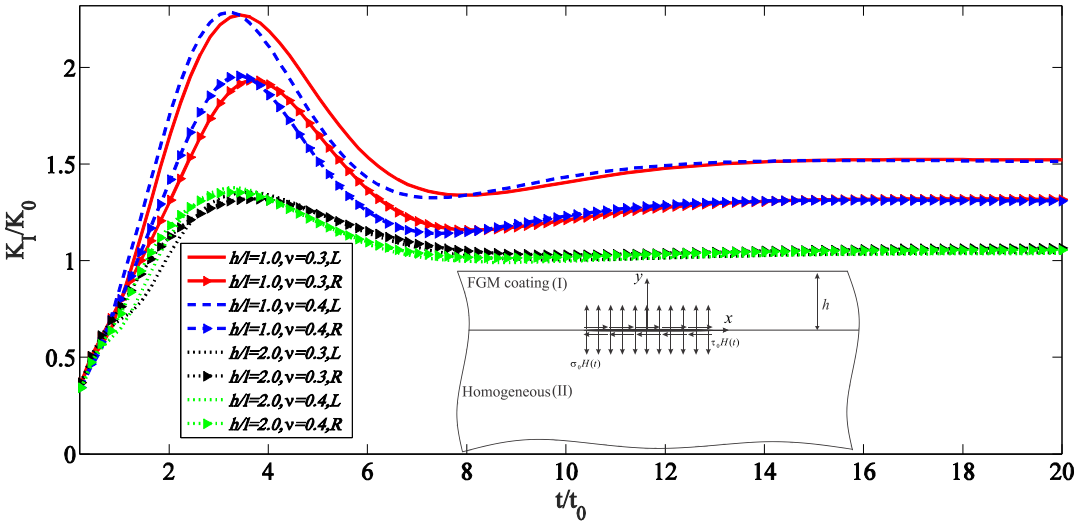

Fig. 12
The influence of Poisson's ratio and coating thickness on transient mode-I DSIFs of an interface crack under mixed mode loading.

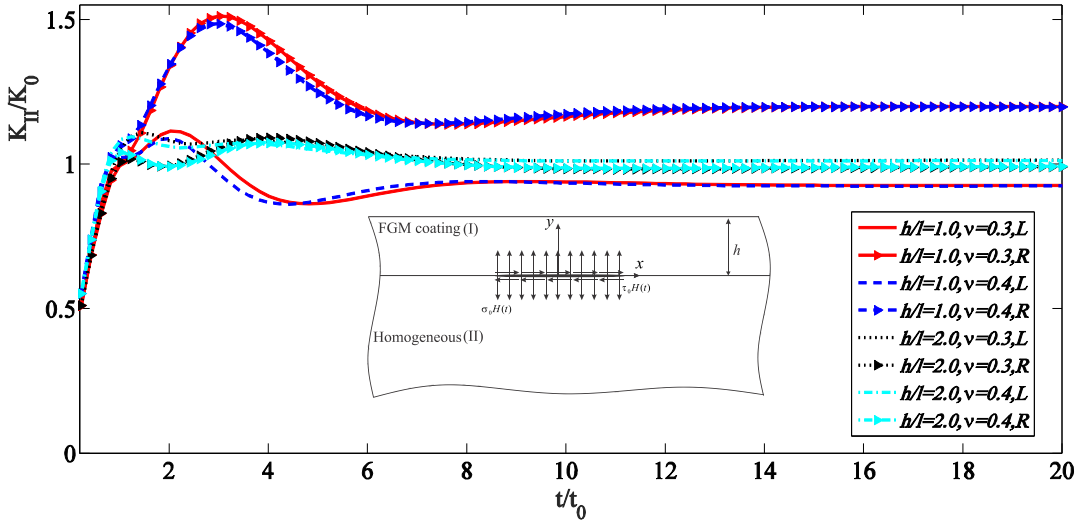

Fig. 13
The impact of Poisson's ratio and coating thickness on transient mode-II DSIFs of an interface crack under mixed mode loading.

Let's delve into the examination of the interaction between multiple cracks. Specifically, we will focus on the interaction between two interface cracks, as portrayed in Figs. (14-17). The next example aim to investigate the interaction between two cracks of equal length under normal loading. The chosen parameters include a coating thickness of $h/l = 2.0$, dimensionless distance $x_{c1}/l = x_{c2}/l = 1.2$, and Poisson's ratio $\nu = 0.3$. In Figure 14, we depict the variations of normalized DSIFs in terms of normalized time t/t_0. It's observable that the DSIFs of two interacting cracks initially reach a peak and subsequently decrease in magnitude until, as t tends to infinity, the results approach the corresponding static values. Remarkably, the DSIFs for the crack tips L_1, R_2 are higher than those for L_2, R_1, which is attributed to the strong interaction. It is also noted that the mode-I DSIFs increase with decreasing nonhomogeneity. Furthermore, when compared to the single crack problem, we observe higher DSIF values due to the interaction effect between the cracks.

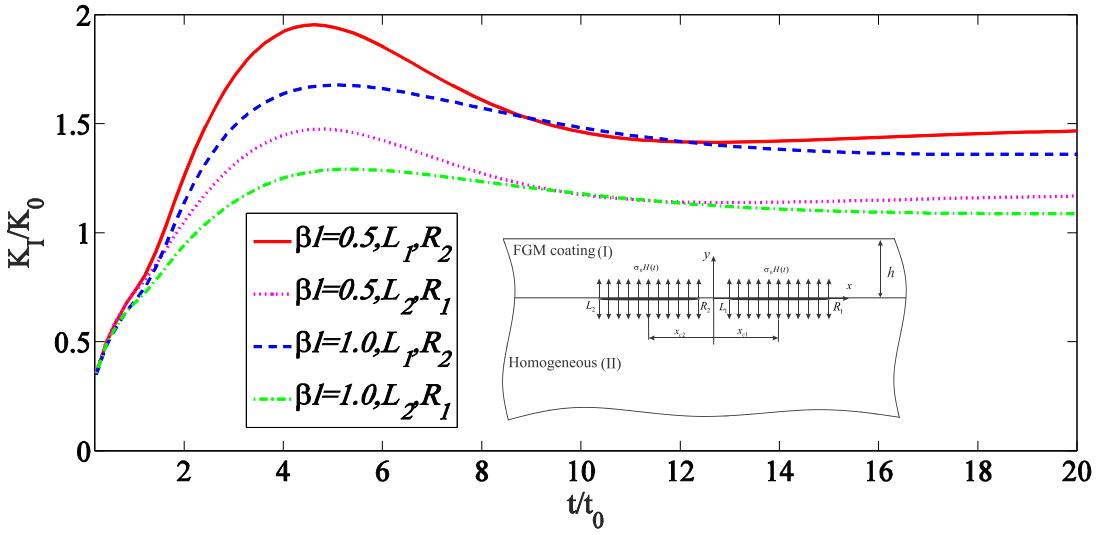

Fig. 14
The effects of two interface cracks on mode-I DSIFs under normal loading.

Following the pattern of the two previous examples, Figure 15 depicts the normalized DSIFs over time (t/t_0) for a pair of identical, equal-length cracks subjected to shear loading. Noteworthy is the observation that the peak values of the crack tips DSIFs in mode II manifest when the nonhomogeneous parameter is reduced.

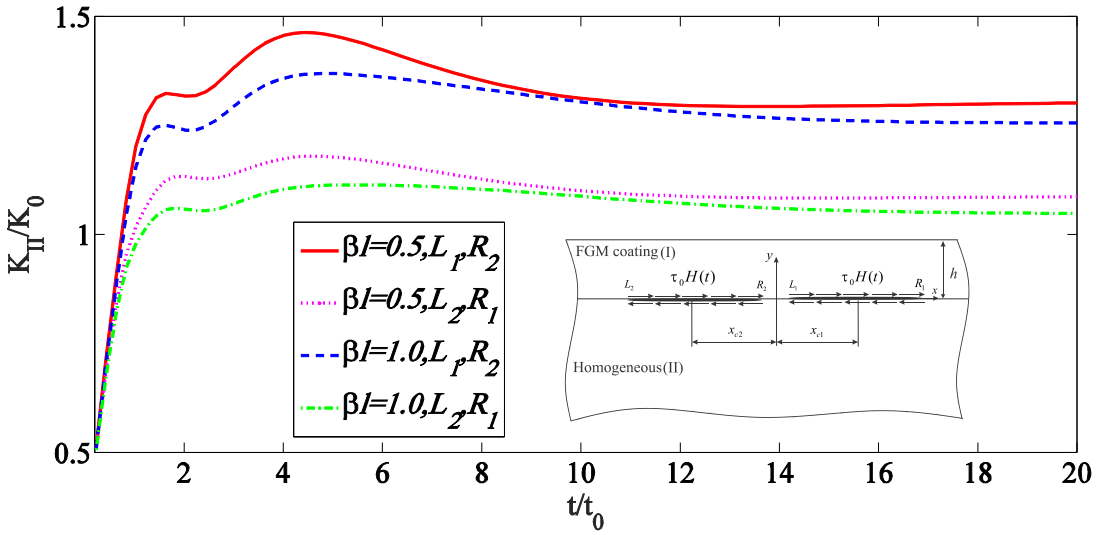

Fig. 15
Cracks behavior at an interface under shear loading: the effects of βl on two mode-II cracks.

Figures 16 and 17 illustrate two equal-length cracks positioned at the interfaces of two mediums. The distance between the centers of these cracks, $x_{c1} = 0.12cm$ and $x_{c2} = -0.12cm$, remains constant while the crack length varies. In these examples, the dimensionless DSIFs are examined in relation to dimensionless time for different crack lengths, specifically $l/x_c = 0.5$ and 0.8. Crack growth is a self-reinforcing phenomenon. As cracks extend, the DSIFs at their tips escalate dramatically. This is further exacerbated by the shrinking distance between the cracks, fostering a complex interaction that propels the DSIFs even higher.

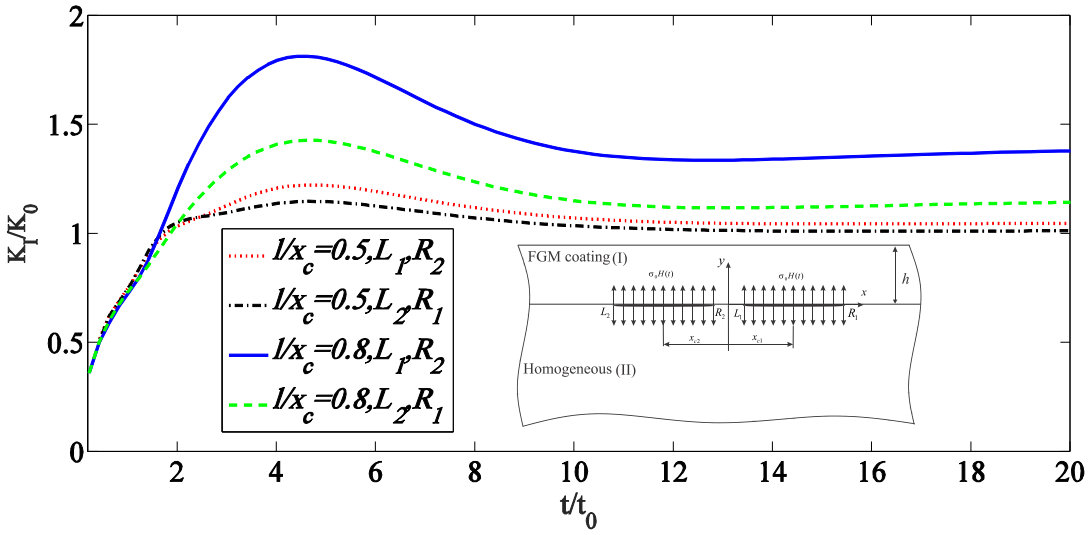

Fig. 16
Crack interaction at an interface under normal loading: the effect of l/x_c on the mode-I DSIFs.

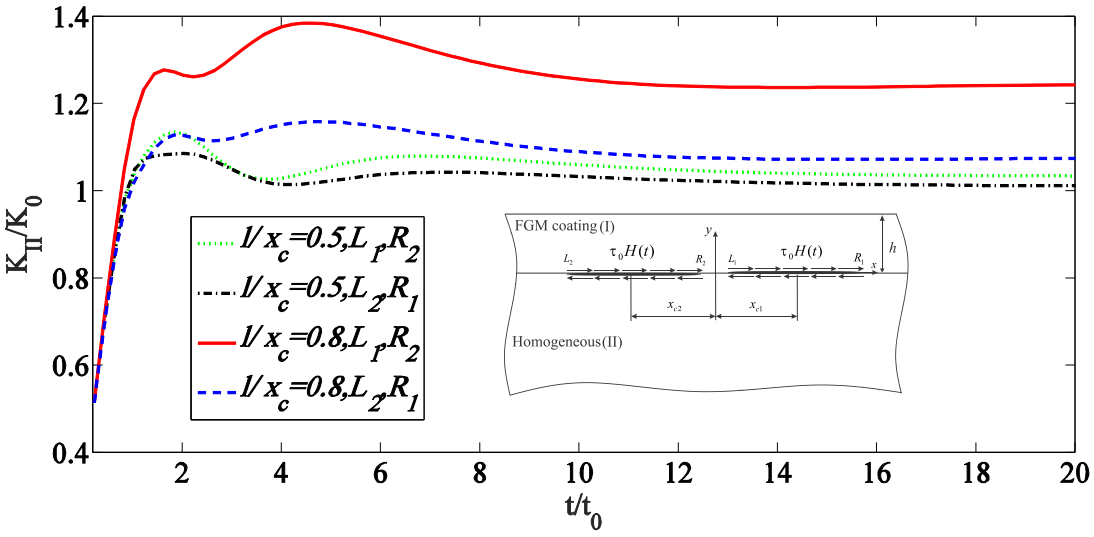

Fig. 17
The interplay of two interface cracks in mode-II under shear loading: the influence of l/x_c .

5 CONCLUDING REMARKS

The effect of mixed-mode impact loading on the behavior of several interface cracks in a homogeneous half-plane with a functionally graded coating is investigated in this study. The material behavior of the coating varies continuously in the transverse direction, while the crack faces experience uniform normal, shear, and mixed-mode loading. To address this complex problem, a system of singular integral equations for the dislocation density is used. The validity of the technique is established through comprehensive validation processes, including the analysis of a single crack in an infinite plane with isotropic material properties, as well as scenarios involving nonhomogeneous elastic half-planes and elastic half-planes subjected to normal impact loading. The findings related to several interface cracks have unveiled the following insights:

(1) The non-uniform material properties have a major impact on the time-dependent stress intensity factors (SIFs), while the Poisson ratio has a minor effect.
(2) The DSIF values for situations involving two cracks exceed those for a single crack. This is due to the coupling between the crack tips of two cracks.
(3) The findings of this study lend credence to the theoretical underpinnings of analytical solutions developed by previous researchers, such as Sih and Embley [24], Mottale et al. [25], and Jafari et al. [26].
(4) The crack length increase is observed to lead to an increase in the maximum DSIFs at the crack tips.
(5) As the length of the two cracks increase, the distance between the two cracks decreases. This leads to an increase in the DSIFs at the tips of both cracks.

NOMENCLATURE

$A_1(s), A_2(s), A_3(s), A_4(s),$ $C_1(s), C_2(s), C_3(s), C_4(s)$	Unknown coefficients
$b_x(t), b_y(t)$	Volterra glide and climb of edge dislocations
$b_{xk}(q,s), b_{yk}(q,s)$	Laplace transform of the dislocation densities
$1/c$	Shear wave velocity
E_0	Elastic modulus
$g_{ki}(q,s), k \in \{x, y\}$	Regular terms of dislocation densities
$H(x)$	Heaviside step function
h	Thickness of FGM| layer
K_I, K_{II}	Dynamic stress intensity factors for Modes I and II
K_0	Stress intensity factor of a crack in infinite plane
$k_{ik}^{1m}(p,q,s), m = 1,2, i, k = x, y$	Kernels of integral equations
l	Half lengths of the crack
N	Total number of cracks
r	Distance from the crack tip
s	Laplace variable
t	Time variable
U, V	Fourier transforms of the displacement component
u, v	In-plane displacement component
x	Spatial variable
$x_i(p), y_i(p)$	Functions describing the geometry of cracks
β	FGM exponent
$\delta(\zeta)$	Dirac delta function
κ	Kolosov constant
μ_0	Elastic constant at the interface
ν	Poisson ratio of the material
$\rho(y)$	Mass density
$\sigma_{xx}, \sigma_{yy}, \tau_{xy}$	In-plane stress components
ζ	Fourier variable

APPENDIX I

The parameters involved in equations (13a) and (13b) are as follows:

$$C_{11}=\frac{b_{23}}{b_{13}-b_{23}}+\frac{(e^{h(\lambda_3+2\lambda_4)}a_{43}(a_{34}a_{43}-a_{33}a_{44}))N_{22}(b_{14}b_{23}-b_{13}b_{24})}{(b_{13}-b_{23})M_{12}}$$
$$+\frac{[\frac{N_{21}M_{12}-N_{22}M_{11}}{(b_{13}-b_{23})M_{12}}](e^{h(\lambda_3+2\lambda_4)}a_{43}(a_{34}a_{43}-a_{33}a_{44}))(M_{12}(b_{11}b_{23}-b_{13}b_{21})-M_{22}(b_{14}b_{23}-b_{13}b_{24}))}{M_{21}M_{12}-M_{22}M_{11}}$$

$$C_{12}=\frac{(e^{h(\lambda_3+2\lambda_4)}a_{43}(a_{34}a_{43}-a_{33}a_{44}))(-N_{21}M_{12}+N_{22}M_{11})}{M_{21}M_{12}-M_{22}M_{11}}$$

$$C_{21}=-\frac{b_{13}}{b_{13}-b_{23}}-\frac{(e^{h(\lambda_3+2\lambda_4)}a_{43}(a_{34}a_{43}-a_{33}a_{44}))N_{12}(b_{14}b_{23}-b_{13}b_{24})}{(b_{13}-b_{23})M_{12}}$$
$$+\frac{[\frac{-N_{11}M_{12}+N_{12}M_{11}}{(b_{13}-b_{23})M_{12}}](e^{h(\lambda_3+2\lambda_4)}a_{43}(a_{34}a_{43}-a_{33}a_{44}))(M_{12}(b_{11}b_{23}-b_{13}b_{21})-M_{22}(b_{14}b_{23}-b_{13}b_{24}))}{M_{21}M_{12}-M_{22}M_{11}}$$

$$C_{22}=\frac{(e^{h(\lambda_3+2\lambda_4)}a_{43}(a_{34}a_{43}-a_{33}a_{44}))(N_{11}M_{12}-N_{12}M_{11})}{M_{21}M_{12}-M_{22}M_{11}}$$

$$A_{11}=-\frac{e^{h(\lambda_3+2\lambda_4)}a_{43}(a_{34}a_{43}-a_{33}a_{44})(M_{12}(b_{11}b_{23}-b_{13}b_{21})-M_{22}(b_{14}b_{23}-b_{13}b_{24})}{M_{21}M_{12}-M_{22}M_{11}}$$

$$A_{12}=\frac{e^{h(\lambda_3+2\lambda_4)}a_{43}(a_{34}a_{43}-a_{33}a_{44})M_{12}(b_{13}-b_{23})}{M_{21}M_{12}-M_{22}M_{11}}$$

$$A_{21}=-\frac{(e^{h(\lambda_3+2\lambda_4)}a_{43}(a_{34}a_{43}-a_{33}a_{44}))(b_{14}b_{23}-b_{13}b_{24})}{M_{12}}$$
$$+\frac{(e^{h(\lambda_3+2\lambda_4)}a_{43}(a_{34}a_{43}-a_{33}a_{44}))(M_{11}M_{12}(b_{11}b_{23}-b_{13}b_{21})-M_{11}M_{22}(b_{14}b_{23}-b_{13}b_{24}))}{M_{12}(M_{21}M_{12}-M_{22}M_{11})}$$

$$A_{22}=-\frac{e^{h(\lambda_3+2\lambda_4)}a_{43}(a_{34}a_{43}-a_{33}a_{44})M_{11}(b_{13}-b_{23})}{M_{21}M_{12}-M_{22}M_{11}}$$

$$A_{31}=\frac{(e^{h(\lambda_2+2\lambda_4)}a_{43}(a_{24}a_{43}-a_{23}a_{44}))(b_{14}b_{23}-b_{13}b_{24})}{M_{12}}$$
$$+\frac{(e^{h(\lambda_1+2\lambda_4)}a_{43}(a_{14}a_{43}-a_{13}a_{44})M_{12}-e^{h(\lambda_2+2\lambda_4)}a_{43}(a_{24}a_{43}-a_{23}a_{44})M_{11})(M_{12}(b_{11}b_{23}-b_{13}b_{21})-M_{22}(b_{14}b_{23}-b_{13}b_{24}))}{M_{12}(M_{21}M_{12}-M_{22}M_{11})}$$
$$A_{32}=-\frac{(e^{h(\lambda_1+2\lambda_4)}a_{43}(a_{14}a_{43}-a_{13}a_{44})M_{12}-e^{h(\lambda_2+2\lambda_4)}a_{43}(a_{24}a_{43}-a_{23}a_{44})M_{11})(b_{13}-b_{23})}{M_{21}M_{12}-M_{22}M_{11}}$$

$$A_{41}=-\frac{(e^{h(\lambda_2+\lambda_3+\lambda_4)}a_{43}(a_{24}a_{33}-a_{23}a_{34}))(b_{14}b_{23}-b_{13}b_{24})}{M_{12}}$$
$$+\frac{(e^{h(\lambda_1+\lambda_3+\lambda_4)}a_{43}(a_{14}a_{33}-a_{13}a_{34})M_{12}-e^{h(\lambda_2+\lambda_3+\lambda_4)}a_{43}(a_{24}a_{33}-a_{23}a_{34})M_{11})(M_{12}(b_{11}b_{23}-b_{13}b_{21})-M_{22}(b_{14}b_{23}-b_{13}b_{24}))}{-M_{12}(M_{21}M_{12}-M_{22}M_{11})}$$
$$A_{42}=\frac{(e^{h(\lambda_1+\lambda_3+\lambda_4)}a_{43}(a_{14}a_{33}-a_{13}a_{34})M_{12}-e^{h(\lambda_2+\lambda_3+\lambda_4)}a_{43}(a_{24}a_{33}-a_{23}a_{34})M_{11})(b_{11}b_{23}-b_{13}b_{23})}{M_{21}M_{12}-M_{22}M_{11}}$$

$$N_{ij}=b_{i3}-a_{j3}+\frac{e^{h(\lambda_j-\lambda_4)}a_{j3}(a_{43}-b_{i3})}{a_{43}}+\frac{e^{h(\lambda_j-\lambda_3)}(a_{j4}a_{43}-a_{j3}a_{44})(-a_{43}b_{i3}+a_{33}(a_{43}+e^{h(\lambda_3-\lambda_4)}(-a_{43}+b_{i3})))}{a_{43}(a_{34}a_{43}-a_{33}a_{44})}$$
$i,j=1,2$

$$M_{1j}=e^{h(\lambda_3+\lambda_4)}(a_{34}a_{43}-a_{33}a_{44})[e^{h\lambda_4}a_{43}((a_{j3}-b_{23})(b_{14}-b_{24})+(b_{13}-b_{23})(-a_{j4}+b_{24}))$$
$$-e^{h\lambda_j}a_{j3}((a_{43}-b_{23})(b_{14}-b_{24})+(b_{13}-b_{23})(-a_{44}+b_{24}))]$$
$$-e^{h(\lambda_j+\lambda_4)}(a_{j4}a_{43}-a_{j3}a_{44})[e^{h\lambda_4}a_{43}((a_{33}-b_{23})(b_{14}-b_{24})+(b_{13}-b_{23})(-a_{34}+b_{24}))$$
$$-e^{h\lambda_3}a_{33}((a_{43}-b_{23})(b_{14}-b_{24})+(b_{13}-b_{23})(-a_{44}+b_{24}))]$$

$$M_{2j}=e^{h(\lambda_3+\lambda_4)}(a_{34}a_{43}-a_{33}a_{44})[e^{h\lambda_4}a_{43}((a_{j3}-b_{23})(b_{11}-b_{21})+(b_{13}-b_{23})(-a_{j1}+b_{21}))$$
$$-e^{h\lambda_j}a_{j3}((a_{43}-b_{23})(b_{11}-b_{21})+(b_{13}-b_{23})(-a_{41}+b_{21}))]$$
$$-e^{h(\lambda_j+\lambda_4)}(a_{j4}a_{43}-a_{j3}a_{44})[e^{h\lambda_4}a_{43}((a_{33}-b_{23})(b_{11}-b_{21})+(b_{13}-b_{23})(-a_{31}+b_{21}))$$
$$-e^{h\lambda_3}a_{33}((a_{43}-b_{23})(b_{11}-b_{21})+(b_{13}-b_{23})(-a_{41}+b_{21}))]$$

REFERENCES

[1] El-Borgi S., Erdogan F., Ben Hatira F., 2003, Stress intensity factors for an interface crack between a functionally graded coating and a homogeneous substrate, *In J Fract* **123:** 139–162.
[2] Chi S., Chung Y.L., 2003, Cracking in coating–substrate composites with multi-layered and FGM coatings, *Eng Fract Mech* **70:** 1227–1243.
[3] Huang G.Y., Wang Y.S., Gross D., 2003, Fracture analysis of functionally graded coatings: plane deformation, *Eur J Mech A/Solid* **22:** 535–544.
[4] Dag S., Yildirim B., Erdogan F., 2004, Interface crack problems in gradedorthotropic media: Analytical and computational approaches, *Int J Fract* **130:** 471–496.
[5] Liu L., Kardomateas G.A., Holmes J.W., 2004, Mixed-mode stress intensity factors for a crack in an anisotropic bi-material strip, *Int J Solids Struct* **41:** 3095–3107.
[6] Huang G.Y., Wang Y.S., Yu S.W., 2005, A new model for fracture analysis of functionally graded coatings under plane deformation, *Mech Mater* **37:** 507–516.
[7] Chen J., 2005, Determination of thermal stress intensity factors for an interface crack in a graded orthotropic coating-substrate structure, *Int J Fract* **133:** 303–328.
[8] Long X., Delale F., 2005, The mixed mode crack problem in an FGM layer bonded to a homogeneous half-plane, *Int J Solids Struct* **42:** 3897–3917.

[9] Guo L.C., Wu L.Z., Zeng T., Ma L., 2004, The dynamic fracture behavior of a functionally graded coating–substrate system, *Compos Struct* **64:** 433–441.
[10] Guo L.C., Wu L.Z., Zeng T., Ma L., 2004, Fracture analysis of a functionally graded coating-substrate structure with a crack perpendicular to the interface-Part II: Transient problem, *Int J Fract* **127:** 39–59.
[11] Guo L.C., Wu L.Z., Zeng T., Cao D., 2005, The transient response of a coating–substrate structure with a crack in the functionally graded interfacial layer, *Compos Struct* **70:** 109–119.
[12] Yong dong L., Bin J., Nan Z., Li qiang T., Yao D., 2006, Dynamic stress intensity factor of the weak/micro-discontinuous interface crack of a FGM coating, *Int J Solids Struct* **43:** 4795–4809.
[13] Guo L.C., Noda N., 2008, Dynamic investigation of a functionally graded layered tructure with a crack crossing the interface, *Int J Solids Struct* **45:** 336–357.
[14] Itou S., 2010, Dynamic stress intensity factors for two parallel interface cracks between a nonhomogeneous bonding layer and two dissimilar elastic half-planes subject to an impact load, *Int J Solids Struct* **47:** 2155–2163.
[15] Vafa J.P., Baghestani A.M., Fariborz S.J., 2015, Transient screw dislocation in exponentially graded FG layers, *Arch Appl Mech* **85:** 1–11.
[16] Vafa J.P., Fariborz S.J., 2016, Transient analysis of multiply interacting cracks in orthotropic layers, *Eur J Mech A/Solids* **60:** 254-276.
[17] Yousefi P., Fariborz J., Fariborz S.J., 2016, Half-layers with interface cracks under anti-plane impact, *Theor Appl Fract Mech* **85:** 367-374.
[18] Fallahnejad M., Bagheri R., Noroozi M., 2018, Transient analysis of two dissimilar FGM layers with multiple interface cracks, *Struct Eng Mech* **67:** 277-281.
[19] Bagheri R., 2019, Transient behavior of multiple interface cracks in two non-homogeneous half-layers, *IJST-T Mech Eng* **44:** 619–629.
[20] Bagheri R., Monfared M.M., 2020, In-plane transient analysis of two dissimilar nonhomogeneous half-planes containing several interface cracks, *Acta Mech* **231:** 3779–3797.
[21] Stehfest H., 1970, Algorithm 368: Numerical inversion of Laplace transforms [D5], *Commun ACM* **13:** 47-49.
[22] Bueckner H., 1958, The propagation of cracks and the energy of elastic deformation, *Transaction of the ASME Series E* **80:** 1225-1230.
[23] Baghestani A.M., Fotuhi A.R., Fariborz S.J., 2013, Multiple interacting cracks in an orthotropic layer, *Arch Appl Mech* **83:** 1549-1567.
[24] Sih G., Embley G., Ravera R., 1972, Impact response of a finite crack in plane extension, *Int J Solids Struct* **8:** 977-993.
[25] Mottale H., Monfared M.M., Bagheri R., 2018, The multiple parallel cracks in an orthotropic non-homogeneous infinite plane subjected to transient in-plane loading, *Eng Fract Mech* **199:** 220-234.
[26] Jafari A., Monfared M.M., Bagheri R., 2019, Mixed‐mode computation of the transient dynamic stress intensity factor for multiple interface cracks, *J Braz Soc Mech Sci* **41:** 573.
[27] Monfared M.M., Ayatollahi M., 2016, Multiple crack problems in nonhomogeneous orthotropic planes under mixed mode loading conditions, *Eng Fract Mech* **155:** 1-17.